








Review

Phantomless Computed Tomography-Based Quantitative Bone Mineral Density Assessment: A Literature Review

Carlo A. Mallio ^{1,2,*}, Daniele Vertulli ^{1,2}, Caterina Bernetti ^{1,2}, Massimo Stiffi ^{1,2}, Federico Greco ³, Johan Van Goethem ⁴, Paul M. Parizel ^{5,6}, Carlo C. Quattrocchi ⁷ and Bruno Beomonte Zobel ^{1,2}

- ¹ Fondazione Policlinico Universitario Campus Bio-Medico, 00128 Rome, Italy; daniele.vertulli@unicampus.it (D.V.); c.bernetti@policlinicocampus.it (C.B.); massimo.stiffi@unicampus.it (M.S.); b.zobel@policlinicocampus.it (B.B.Z.)
- ² Research Unit of Radiology, Department of Medicine and Surgery, Università Campus Bio-Medico di Roma, 00100 Rome, Italy
- ³ Department of Radiology, Cittadella della Salute Azienda Sanitaria Locale di Lecce, 73100 Lecce, Italy; federicogreco@outlook.com
- ⁴ Department of Radiology, Antwerp University Hospital, 2650 Edegem, Belgium; johan.vangoethem@uantwerpen.be
- ⁵ Royal Perth Hospital (RPH), Perth, WA 6001, Australia; paul.parizel@health.wa.gov.au
- ⁶ Medical School, University of Western Australia (UWA), Perth, WA 6009, Australia
- ⁷ Centre for Medical Sciences-CISMed, University of Trento, 38100 Trento, Italy; carlo.quattrocchi@unitn.it
- * Correspondence: c.mallio@policlinicocampus.it; Tel.: +39-06-225411708

Abstract: The global surge in aging populations has intensified osteoporosis challenges, necessitating improved diagnostic methods. While dual X-ray absorptiometry (DXA) is the conventional standard in assessing bone mineral density (BMD), the exploration of quantitative computed tomography (QCT) has been proposed, particularly phantomless techniques. Challenges in single-energy CT, emphasizing internal calibration standards like subcutaneous fat, are discussed. Advances in PL-QCT, notably with automatic region of interest (ROI) selection, show improved accuracy. Dual-energy CT (DECT) introduces new dimensions for musculoskeletal analysis. Despite advancements, challenges persist, including interindividual variability and patient-specific factors. Evolving single-energy CT and DECT techniques show promise in refining BMD assessment and osteoporosis diagnosis, enhancing patient care. Continued research and integration into clinical practice are vital for realizing these advancements' full benefits. In this review, we evaluate and summarize current evidence on the feasibility and different approaches to achieve analysis of BMD with phantomless QCT.

Keywords: CT; bone mineral density; dual energy; osteoporosis; fractures



Citation: Mallio, C.A.; Vertulli, D.; Bernetti, C.; Stiffi, M.; Greco, F.; Van Goethem, J.; Parizel, P.M.; Quattrocchi, C.C.; Beomonte Zobel, B. Phantomless Computed Tomography-Based Quantitative Bone Mineral Density Assessment: A Literature Review. *Appl. Sci.* **2024**, *14*, 1447. <https://doi.org/10.3390/app14041447>

Academic Editor: Rossella Bedini

Received: 13 January 2024
Revised: 5 February 2024
Accepted: 8 February 2024
Published: 9 February 2024



Copyright: © 2024 by the authors. Licensee MDPI, Basel, Switzerland. This article is an open access article distributed under the terms and conditions of the Creative Commons Attribution (CC BY) license (<https://creativecommons.org/licenses/by/4.0/>).

1. Introduction

In recent decades, global aging has outpaced historical trends, especially in developed nations, assisted by improved living conditions and advancements in medicine, that contribute to longer lifespans. This shift is significantly impacting healthcare systems as age-related pathologies surge, including osteoporosis. Osteoporosis is a systemic skeletal disorder characterized by reduced bone mineral density and microarchitectural deterioration of bone tissue, often associated with aging, hormonal changes, and inadequate bone formation [1,2].

Elderly individuals with osteoporosis are burdened by an elevated risk of experiencing fragility fractures after minor trauma, which is a primary contributor to reduced mobility and vulnerability among aging cohorts [3,4]. Prevention strategies include a balanced diet rich in calcium and vitamin D, regular weight-bearing exercise, and pharmacological interventions aimed at preserving bone mass [1,2]. Since pharmacological prevention only accounts for about 5% of the costs associated with osteoporosis [5] and considering that managing complications like fractures is considerably more challenging and costly, there

is a heightened necessity and convenience for early identification of individuals at risk of developing osteoporosis. Achieving an early diagnosis and understanding the molecular and genetic factors contributing to osteoporosis are crucial for developing targeted therapies and improving overall bone health.

In 1994, the World Health Organization proposed, dual X-ray absorptiometry (DXA) as the gold standard for the diagnosis of osteoporosis [6,7] (Figure 1). To date, DXA is a widely accessible, well-standardized technique that quantifies bone mineral density (BMD- g/cm^2) using two X-ray beams of different energies. Nevertheless, several studies have demonstrated that DXA's results can be hindered in assessing BMD [8], due to body composition variations, overlying soft tissue, and vascular calcification, which can cause distortions in the measurements [9–12].

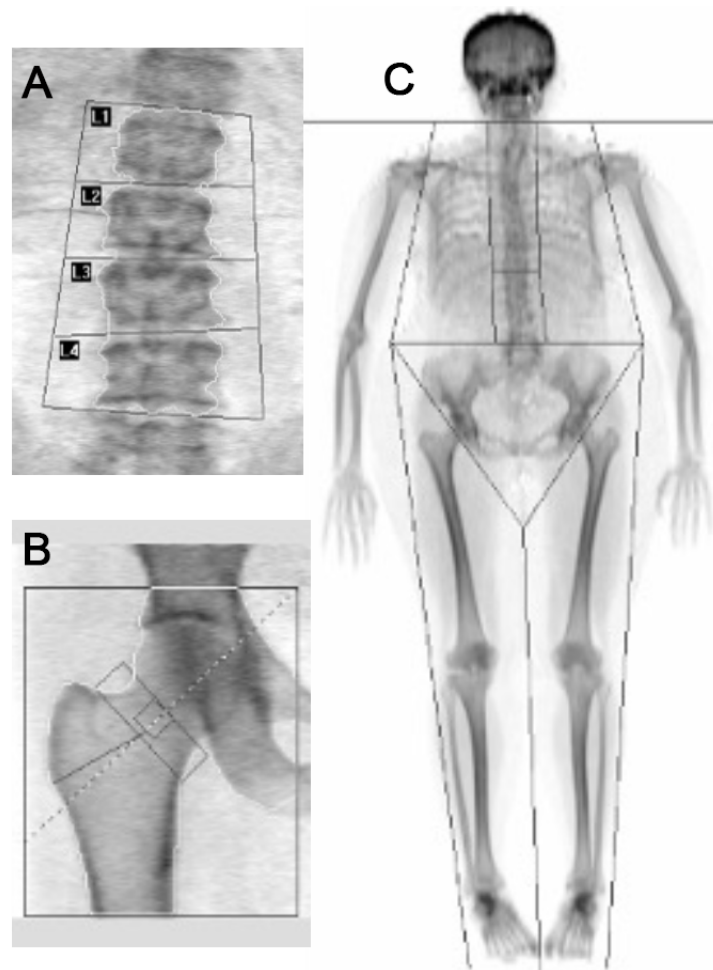


Figure 1. Dual-energy X-ray absorptiometry (DXA) for measuring BMD of the spine at the level of L1–L4 (A), femoral neck (B), and whole body (C).

Clinical practice has relied on DXA to assess bone strength through the typical BMD in a specific region. However, because DXA also ignores 3D bone structure, the representative BMD cannot be a great standalone indicator of bone strength. Several reports have demonstrated that diverse bone architectures in patients with the same BMD might lead to different fracture risks.

Some of these issues might potentially be solved by quantitative computed tomography (QCT), particularly by measuring the volumetric BMD of trabecular bone. This technique makes it easier to analyze localized BMD since it can distinguish between cortical and trabecular bone [13], and it also offers a precise volumetric BMD quantification measured in mg/cm^3 rather than g/cm^2 units [13,14]. Moreover, QCT tests are not affected

by common para-physiologic conditions, often observed in the elderly, such as osteophyte or aortic calcification [15].

The main limit is that these measurements cannot be applied retroactively, but rather they must be performed using calibration phantoms [16–19]. Phantom-based QCT (PB-QCT), which encompasses synchronously calibrated QCT and asynchronously calibrated QCT, and phantomless QCT (PL-QCT) are the two primary categories of QCT. The PB-QCT examination requires a reference phantom made of materials such as K_2HPO_4 with known densities to accurately quantify the BMD values. In contrast to PB-QCT, PL-QCT does not require simultaneous scanning of the external phantom to assess BMD.

The aim of the review is to evaluate the feasibility and different approaches applied to achieve QCT BMD assessment with the phantomless calibration techniques. Being that to the end of predicting the risk of osteoporotic fractures, the most important feature is the detailed assessment of trabecular BMD, we decided to focus our paper on the analysis of trabecular bone.

2. Materials and Methods

In July 2023, two researchers (C.A.M., 12 years of experience, and D.V., 4 years of experience) employed National Library of Medicine databases, including PubMed, NLM catalog, MeSH, and Bookshelf, for the research using the following keywords: “phantomless quantitative”. Titles and abstracts of all the papers were analyzed by the two researchers. Papers were included for further in-depth review if the focus was on PL-QCT to investigate osteoporosis or osteopenia (Figure 2). The references of the eligible studies were screened manually to identify additional studies of potential interest. The characteristics and major findings of the studies included are summarized in Tables 1 and 2.

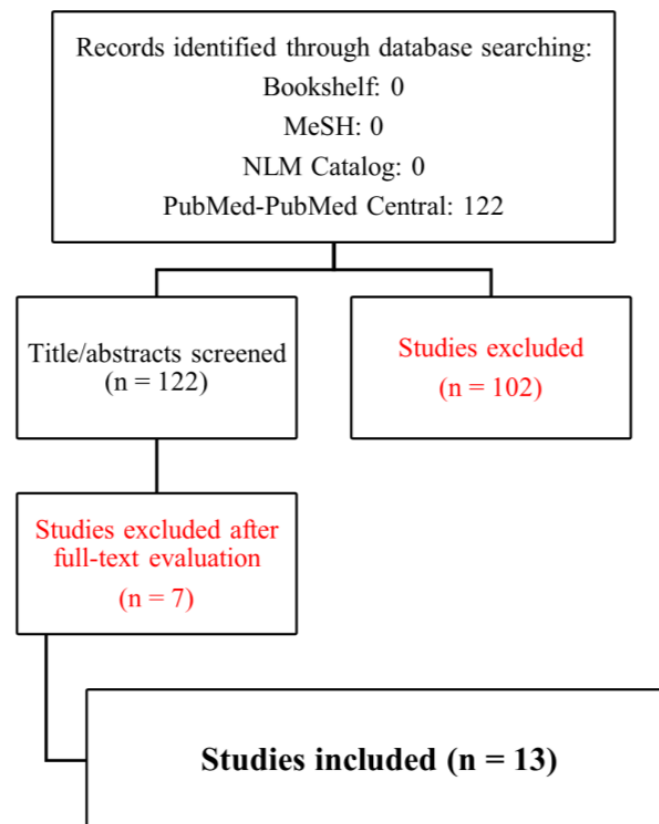


Figure 2. Flowchart for study search and selection.

Table 1. Main characteristics and findings of the analyzed single-energy CT studies included in the review.

Year	First Author	Technique	Results
2010	Mueller et al.	PB-BMD vs. PL-BMD T12–L4	A minor BMD bias of 0.9 mg/cm ³ for the PL-BMD option was found
2011	Pickhardt et al.	T12–L5 levels assessed using both PL-QCT and straightforward non-angled ROI MDCT attenuation measures	For BMD screening at CTC, both PL-QCT and straightforward ROI attenuation measurements of the lumbar spine are useful, with excellent sensitivity for osteoporosis as determined by the DXA T-score
2015	Weaver et al.	PB-QCT vs. PL-QCT approach in L1–L5	Excellent agreement was seen in the linear regression of lumbar vBMD produced from the PB vs. PL calibrations
2017	Lee et al.	Spine and hip analysis using air and either hip adipose tissue or aortic blood as calibrating reference materials	Calibrated measurements using phantoms and PL were equivalent
2018	Therkildsen et al.	PL internal tissue calibration performed on 3 consecutive vertebrae from T12 to L4	The PL technique has a higher intra-operator variability (5.8%) than the PB method (0.8%) and a higher inter-operator variability (5.8%) than the PB method (1.8%)
2019	Lee et al.	PL HU-to-BMD conversion using a multiple linear regression model	Significant correlations between the BMD values calculated using the suggested HU-to-BMD conversion and those obtained using the reference phantom
2022	Liu et al.	Newly developed automatic PL-QCT system	According to the findings of the BMD test, the autonomous PL-QCT system exhibited more precision than earlier studies that used QCT while still being able to detect osteoporosis similarly to DXA and PB-QCT
2022	Xiongfeng et al.	PL-QCT system	PL-QCT can predict osteoporosis with a fair amount of precision and accuracy
2023	Pan et al.	QCT using CNN	The proposed-method-measured BMDs were higher than QCT-measured BMDs in a cohort of study
2023	Di et al.	PL-QCT using automatic calibration technique	Preoperative BMD was an independent risk factor for postoperative cage subsidence after extreme lateral interbody fusion

Table 2. Main characteristics and findings of the analyzed dual-energy CT studies included in the review.

Year	First Author	Technique	Results
2015	Wichmann et al.	Dedicated post-processing	The vertebral pedicle can be evaluated for PL-BMD using quantitative DECT; in comparison to other segments, BMD of the intra-pedicular segment correlates with pedicle screw pull-out strength much more strongly
2020	Booz et al.	DECT post-processing software using material decomposition of L1–L4	Based on volumetric DECT and HU analyses, the overall patient-based AUC was 0.930 vs. 0.79 ($p < 0.001$)
2021	Gruenewald et al.	DECT post-processing software using material decomposition of L1	DECT-derived BMD was substantially linked to the development of new fractures (OR: 0.871)

3. Discussion

3.1. Single-Energy CT

Single-energy CT utilizes a single X-ray energy level to generate detailed anatomical images by measuring tissue attenuation [20,21]. Its applications range from diagnostic imaging to quantitative analysis, providing valuable insights into tissue composition and pathology [20,21].

Before performing any quantitative analysis, it is important to consider all the factors that may impact CT Hounsfield Unit (CTHU) stability, such as the type of scanner used, the patient's body size, and all the parameters for the scan algorithm. One way to reduce errors is by using the subcutaneous fat and paraspinal muscle as internal calibration standards.

Therkildsen et al. [22], by using two different approaches, compared the agreement and precision of BMD measurements: in a cohort of patients with chronic kidney disease, asynchronous PB calibration and PL internal tissue calibration were used. For the latter, a similar approach to the one described for the PB assessment was used to manually place elliptical volumes of interest (VOIs) in the front portion of the mid-vertebral body. On each image, VOIs of muscle and fat were positioned on the right side within the posterior subcutaneous fat, and on the left, within the paraspinal muscle group. The objective was to produce a normal distribution on the HU histogram with a prominent Gaussian fit within the predetermined values. The variable HU distribution inside the muscle and fat ROI could be a drawback. As muscle CT numbers rely on the patient's level of hydration, other variables that might affect accuracy and precision include differences in the patient's vasculature and cellularity. It was found that the measured BMD with phantoms was higher than the measured BMD without phantoms. Despite a negligible absolute difference of 3.3 mg/cm^3 and a negligible relative difference of 5.1%, interindividual variances were substantial. In comparison to the PB approach, the PL methodology exhibits a higher intra- and inter-operator variability. Although there were several connections between the techniques, each person's between-method difference varied greatly.

Due to the manual selection of the region of interest (ROI) of body tissues in the conventional PL-QCT system, its repeatability could be rather low. One significant issue with the conventional PL-QCT is solved by the automatic selection of the ROI for fat and muscle. This process also increases the accuracy of the BMD data by computing BMD values using the calibration factor.

Liu et al. [23] used this innovative system with automatic ROI selection, which makes BMD testing easier, dramatically increasing accuracy if compared to conventional BMD measuring techniques. In a work of Lee et al. [24], the automated ROI technique was used to calibrate the findings of the BMD measurement using the subcutaneous fat and paraspinal muscle as internal calibration standards. Several methods were used to successfully select body tissue ROIs from CT images. First, to accomplish segmentation of various body tissues in CT images, the HU scale was used. As reported by the authors, the determination of the HU range was based on clinical practices and experts' observations of spinal CT scans: fat ($HU_{\min} = -150$; $HU_{\max} = -50$) and muscle ($HU_{\min} = 20$; $HU_{\max} = 80$). Each patient had two or three vertebrae examined, with L1–L3 of major consideration. In the PB-QCT study, an ROI with a restricted range of adjustment was chosen for each vertebra. The anterior portion of the vertebral body was automatically assigned an elliptical VOI, which was then manually modified as needed. The posterior venous plexus and any specific disease, such as bone islands and calcified herniated disks, were avoided to obtain the most accurate values. On each picture, VOIs of muscle and fat were positioned in almost the same locations: on the right side, in the posterior subcutaneous fat, and on the left, in the paraspinal muscle group. For the best match, the VOI's size and form for muscle and fat were modified to produce a normal distribution on the HU histogram with a dominating Gaussian fit within the predetermined values.

Similar PL-QCT was used by Xiongfeng et al. [25], with the automatic function of selecting vertebrae, hip, fat, and muscle ROIs and using fat and muscle ROI CT values to calibrate BMD results with high precision.

For the five different mineral compositions of the reference phantom that were captured in the same CT scans, Lee et al. [26] employed five ROIs. The multiple regression models were used to create the PL HU-to-BMD conversion equations using a stepwise regression technique. The dependent variables were the HU value, circumference, and bone area; the BMD value was the independent variable. The images of the spine and hips were initially segmented. As post-processing, holes were filled, and surfaces were smoothed. The segmented pictures were then instantly transformed from each voxel to a matching 8-node solid element. Using the BMD modulus connection for the spine and femur, the elastic moduli of each finite element were converted from the estimated and reference BMD values of each voxel.

Since the attenuation factor of the patient's soft tissue (psoas and fat) is significantly different from that of bone, using body anatomical markers may affect accuracy. For most contemporary scanners, the calibration factor (ratio in actual density phantom rod and CTHU, $\text{mg}/\text{cm}^3/\text{CTHU}$) was developed, and it could be helpful for assessing BMD.

Mueller et al. [27] discussed the integration of PL-BMD devices into non-dedicated QCT scans of thoracic and abdominal areas, in a head-to-head PB-BMD vs. PL-BMD calculation. With a 9 mm high cylinder to provide a constant VOI, the program automatically placed the elliptic ROI into the trabecular bone compartment of each vertebra. Each tissue ROI's CT number was computed under the assumption of a normal distribution. The program defined the histogram to represent the major tissue component, considering the variable levels of interstitial fat inside the muscle ROI. They concluded that, although PL-BMD's accuracy is less accurate than that of PB-BMD systems, it is a reliable clinical tool for detecting decreased BMD over a wide patient group.

In the study by Pickhardt et al. [28], oval ROIs are positioned on the vertebral body, paraspinal musculature, and subcutaneous fat at each level from T12 to L5, respectively, during PL-QCT. The transverse plane of section is angled to be parallel with the end plate at each level using a sagittal reconstruction. The basivertebral venous plexus posteriorly, the surrounding cortical bone, and any localized lytic or sclerotic lesion are all avoided while placing the vertebral body ROI in the anterior trabecular area. Software generates a BMD measurement (in gm/cc), which was utilized as the primary QCT outcome measure for comparison with the DXA T-score. At L1, a trabecular ROI attenuation cut-off of 160 HU was 100% sensitive (29/29) and 46.4% specific (104/24) for osteoporosis. Area under the curve for osteoporosis using trabecular ROIs at single lumbar levels was 0.888 for PL-QCT and ranged from 0.825 to 0.853.

In a study by Weaver et al. [29] L1–L5 HU values were converted to mg/cc using linear regressions between the mean HU values obtained from the phantom ports and the known mg/cc values. To produce a conversion for L1–L5 HU measurements to mg/cc , a PL calibration approach was established, where the fat and muscle HU values were linearly regressed against the ground truth values for fat (69 mg/cc) and muscle (77 mg/cc). For the 50 participants, the mean lumbar volumetric BMD (vBMD) estimated using the two methods (QCT vs. PL) was compared to determine agreement. Excellent agreement was seen in the linear regression of lumbar vBMD produced from the QCT vs. PL calibrations ($p = 0.0001$). The PL approach can be widely used to both prospectively and retrospectively measure patient bone quality for research and clinical investigations related to motor vehicle crash injuries, falls, and aging, especially since lumbar vBMD was computed from PL-QCT scans with accuracy comparable to QCT.

In another recent study, 1175 participants had QCT for both BMD and low-dose chest CT. For vertebral body segmentation and labeling, two convolutional neural network (CNN) models were used, respectively. Vertebral BMD was calculated using a histogram approach, with paraspinal muscle and surrounding fat serving as references [30].

By using the subcutaneous fat and paraspinal muscle as internal references and automatically setting their coordinate ROIs for BMD calibration, a recent study accomplished the aim of predicting cage placement after extreme lateral interbody fusion [31]. The authors used the following steps to assess the analysis: the best muscle and fat ROIs were

automatically placed for calibration based on a priority algorithm in locations closer to the vertebrae position provided by the user; the segmentation of muscle and fat tissue was performed using an HU range; and followed by the construction of a convolution map based on a kernel pyramid for better tissue boundary robustness. The authors reported that the PL-QCT system can improve the accuracy of vBMD measurements, possibly contributing to the evaluation of patients who underwent cage placement after extreme lateral interbody fusion [31].

The studies included emphasize the challenges related to CTHU variance among scanners, particularly in the context of BMD measurement. Various calibration methods are explored, ranging from manual to automatic ROI selection, with a particular focus on enhancing accuracy through innovative techniques like asynchronous PB calibration and PL internal tissue calibration. The adoption of automatic ROI selection is proposed as a pivotal strategy to improve the precision and repeatability of BMD measurements, showcasing the potential of these advancements for reliable clinical applications in detecting decreased BMD across diverse patient groups.

3.2. Dual-Energy CT

DECT is a more recent imaging modality, which concurrently captures images at two distinct energy levels, enabling refined tissue characterization [32,33]. Widely applied for material decomposition and virtual non-contrast imaging, it also enhances lesion detection and characterization [32,33]. Its diverse applications make it a valuable tool across medical disciplines, contributing to more precise diagnostic capabilities in scientific research. In contrast to traditional CT, material distinction in DECT can provide novel, pertinent information for several musculoskeletal applications [34,35]. A DECT-based post-processing algorithm has recently been evaluated, allowing PL volumetric BMD assessment of lumbar trabecular bone. The accuracy of PL volumetric DECT BMD evaluation based on lumbar spine material breakdown, as an indication for the 2-year occurrence risk of osteoporosis-associated fractures, was studied retrospectively by Gruenewald et al. [36]. They first characterized the trabecular VOI in 3D, prior to performing a PL vBMD evaluation of the L1 vertebra. The whole vertebral body's trabecular bone—not cortical bone—was included in the VOI for this analysis. The VOI and the two DECT series (90 and 150 kVp) were loaded into a second measure of the volumetric BMD.

The algorithm uses specialized material breakdown to identify between each voxel's collagen matrix, calcium hydroxyapatite, water, fat marrow, and adipose tissue composition, as exposed in a previous work by Nickoloff et al. [37]. They employed a biophysical model-based technique that considered the five main components of trabecular bone. The fraction of the volume occupied by the matrix material (i.e., bone mineral + collagen), V_{TB} , and the volume of fat tissue, V_F , are related to the HU intensities of both imaging data sets at 90 and 150 kV. The remaining variables are energy-related constants, and the values for t and g are 0.92 and 1.02, respectively. Therefore, values for V_{TB} and V_F can be acquired by calculating the mean intensity for an area of the trabecular bone in both imaging data sets, and the BMD value BM expressed in g/cm^3 can be determined from V_{TB} .

Using a similar approach, Booz et al. [38] identified the trabecular VOI of each vertebra, not only L1 like the previous study, but from L1 to L4. The selected VOI was the whole vertebral body's trabecular bone, carefully excluding the cortical bone. The VOI and the two DECT series (90 and 150 KVp) were used as input for the volumetric BMD evaluation. A second step was to distinguish among red blood cells, water, collagen matrix, bone minerals, and adipose tissue for each voxel, was used to perform volumetric BMD evaluation.

For PL assessment of the cancellous BMD of vertebral pedicles and to investigate the relationship with pedicle screw pull-out strength, Wichmann et al. [39] examined the quantitative DECT. First, a template mesh representing each pedicle screw vector in the 3D image data set was automatically added using an automated method for recognizing vertebral anatomy. The user then evaluated this template mesh to determine how to appropriately exclude cortical bone and delineate the cancellous pedicle screw vector

and, if necessary, manually deform it. The labeled volume and the two image data sets corresponding to the low-energy and high-energy DECT scans were then imported into the analysis application.

According to the calculated spatial cancellous BMD distribution for all indicated locations, each voxel in the bone region considered of each pedicle vector was assigned a unique BMD value. Both a global value for the whole pedicle screw vector and particular values for each pedicle segment were calculated. The 3D representation of the estimated spatial distribution of cancellous BMD values in the resultant pedicle screw vector was shown and overlaid on the vertebral model. Red indicates places with low BMD, white areas with normal BMD, and blue areas with high BMD. They concluded that the vertebral pedicle can be evaluated for PL-BMD using quantitative DECT. In comparison to other segments, BMD of the intrapedicular segment correlated with pedicle screw pull-out strength much more strongly.

DECT, capturing images at two energy levels, proves invaluable for precise tissue characterization and material decomposition in musculoskeletal applications. Recent advancements include a DECT-based algorithm for lumbar trabecular bone assessment, demonstrating potential in predicting the 2-year risk of osteoporosis-associated fractures. Automated PL-QCT programs and quantitative DECT analysis further enhance accuracy in BMD measurements, offering a comprehensive approach for clinical evaluation and research in the field of bone health.

4. Future Perspectives: Artificial Intelligence

In the rapidly evolving landscape of osteoporosis diagnosis and imaging, future perspectives hold promising developments, particularly with the integration of advanced technologies such as artificial intelligence (AI). This is a branch of computer science focused on developing systems that can perform tasks that typically require human intelligence [40–43]. In various fields, AI algorithms analyze data, learn patterns, and make predictions, offering solutions ranging from image recognition and natural language processing to complex problem solving. In healthcare, AI is increasingly utilized for diagnosis, prognosis, and treatment optimization, showcasing its potential to enhance efficiency and accuracy in medical applications [44–46].

DECT, as discussed earlier, showcases potential for precise osteoporosis risk assessment. Incorporating AI algorithms into DECT analysis could further refine predictive models, leveraging machine learning to enhance fracture risk predictions based on intricate bone composition details captured by DECT. On the other hand, strategies applied to single-energy CT can have broader and more extensive applications, including the analysis of already acquired images and follow-up assessments. Furthermore, ongoing research, as exemplified by Gruenewald et al., emphasizes the potential of DECT-based algorithms for volumetric BMD assessments [36]. The automated identification of trabecular bone components and the application of biophysical models could revolutionize BMD evaluations, offering more nuanced insights into bone health and fracture susceptibility. On this perspective, the integration of AI into traditional and advanced imaging modalities opens avenues for automated ROI selection, precise material breakdown, and improved diagnostic accuracy, possibly streamlining the assessment process, reducing the time-consuming nature, and ensuring consistency across multiple regions [41,47].

Opportunistic osteoporosis screening could be performed on CT images acquired for other purposes. On this respect, Yang et al. recently reported, using an AI-based solution, that attenuation values in thoracic and first lumbar vertebrae, particularly in menopausal women, showed a strong correlation with osteopenia and osteoporosis risk. A 10 HU increase in CT values significantly reduced this risk. The combined diagnostic efficacy of all thoracic vertebrae surpasses that of a single vertebra, providing a valuable, radiation-efficient method to identify, using the opportunistic approach, high-risk individuals, possibly reducing fracture incidence [48].

Another recent and intriguing perspective involves a predictive model designed to detect osteoporosis using radiomic features extracted from lumbar spine CT images [49].

This radiomic model demonstrated excellent performance, with an area under the curve of 0.994 (95% confidence interval: 0.979–1.00), effectively distinguishing between normal BMD and osteoporosis in lumbar spine CT images [49].

Moreover, AI can be applied also to MRI to detect osteoporosis. For instance, Ferizi et al. reported the results of a prospective case—control study involving women with and without fragility bone fractures that employed 15 machine learning classifiers on 3T 3D FLASH MRI data [50]. This study underscored the potential of machine learning in predicting osteoporosis and fractures on MRI.

Looking ahead, the use of AI in osteoporosis imaging is not only limited to diagnostic applications but extends to predictive analytics. As technological capabilities advance, AI models may evolve to predict individualized fracture risk based on comprehensive imaging data, patient demographics, and clinical history.

Consideration should also be given to recent technical developments in imaging acquisition. On this respect, there have been recent attempts to diagnose osteoporosis using MR-based proton density fat fraction (PDFF) measurements. In a recent study, CT-based HU values demonstrated good performance and PDFF showed fair performance to diagnose osteopenia and osteoporosis, suggesting that PDFF also could be used to investigate BMD without exposure to ionizing radiation [51].

In summary, the future of osteoporosis imaging holds significant promise with the integration of artificial intelligence, particularly in refining diagnostic accuracy, automating analysis processes, and advancing predictive modeling.

5. Conclusions

The present review explores recent advancements in QCT and DECT. PL-QCT techniques, both single- and dual-energy, emerge as promising tools for accurate BMD assessments in addition to the traditional bone density assessment methods, such as DXA. Moreover, the integration of AI holds transformative potential, enhancing diagnostic accuracy and predictive modeling. The convergence of AI with advanced imaging technologies, like DECT, offers a path toward personalized and effective osteoporosis management strategies in the future. Additional research is required to pinpoint the most effective imaging strategy for detecting osteoporosis, ensuring a thorough understanding of the topic.

Author Contributions: Conceptualization, C.A.M. and D.V.; methodology, C.A.M. and D.V.; software, C.A.M. and D.V.; validation, All authors; formal analysis, All authors; investigation, All authors; resources, C.A.M. and D.V.; data curation, C.A.M. and D.V.; writing—original draft preparation, C.A.M. and D.V.; writing—review and editing, All authors; visualization, All authors; supervision, B.B.Z.; project administration, All authors. All authors have read and agreed to the published version of the manuscript.

Funding: This research received no external funding.

Conflicts of Interest: The authors declare no conflicts of interest.

Abbreviations

3D	Three-dimensional
BMD	Bone mineral density
CT	Computed tomography
CTHU	Computed tomography Hounsfield Unit
DXA	Dual X-ray absorptiometry
PB	Phantom-based
PL	Phantomless
PB-BMD	Phantom-based BMD
PLBMD	Phantomless BMD
PB-QCT	Phantom-based QCT
PL-QCT	Phantomless QCT
QCT	Quantitative computed tomography

QDECT	Quantitative dual-energy CT
ROI	Region of interest
vBMD	Volumetric bone mineral density
VOI	Volume of interest

References

- Akkawi, I.; Zmerly, H. Osteoporosis: Current Concepts. *Joints* **2018**, *6*, 122–127. [[CrossRef](#)] [[PubMed](#)]
- Sozen, T.; Ozisik, L.; Calik Basaran, N. An Overview and Management of Osteoporosis. *Eur. J. Rheumatol.* **2017**, *4*, 46–56. [[CrossRef](#)] [[PubMed](#)]
- Hernlund, E.; Svedbom, A.; Ivergård, M.; Compston, J.; Cooper, C.; Stenmark, J.; McCloskey, E.V.; Jönsson, B.; Kanis, J.A. Osteoporosis in the European Union: Medical Management, Epidemiology and Economic Burden. *Arch. Osteoporos.* **2013**, *8*, 136. [[CrossRef](#)] [[PubMed](#)]
- Mallio, C.A.; Beomonte Zobel, B.; Quattrocchi, C.C. Evaluating Rehabilitation Interventions in Parkinson's Disease with Functional MRI: A Promising Neuroprotective Strategy. *Neural Regen. Res.* **2015**, *10*, 702. [[CrossRef](#)] [[PubMed](#)]
- Kanis, J.A.; Svedbom, A.; Harvey, N.; McCloskey, E. V The Osteoporosis Treatment Gap. *J. Bone Miner. Res.* **2014**, *29*, 1926–1928. [[CrossRef](#)] [[PubMed](#)]
- Jain, R.K.; Vokes, T. Dual-Energy X-ray Absorptiometry. *J. Clin. Densitom.* **2017**, *20*, 291–303. [[CrossRef](#)] [[PubMed](#)]
- Jiang, Y.; Wu, Y.; Zhang, Y.; Yang, X.; Gao, J. A Cross-Calibration Study Using a Novel Dual X-Ray Absorptiometry System for Bone Mineral Density Measurements with the European Spine Phantom. *Quant. Imaging Med. Surg.* **2023**, *13*, 2119–2127. [[CrossRef](#)]
- Schuit, S.C.E.; van der Klift, M.; Weel, A.E.A.M.; de Laet, C.E.D.H.; Burger, H.; Seeman, E.; Hofman, A.; Uitterlinden, A.G.; van Leeuwen, J.P.T.M.; Pols, H.A.P. Fracture Incidence and Association with Bone Mineral Density in Elderly Men and Women: The Rotterdam Study. *Bone* **2004**, *34*, 195–202. [[CrossRef](#)]
- Bolotin, H.H. DXA in Vivo BMD Methodology: An Erroneous and Misleading Research and Clinical Gauge of Bone Mineral Status, Bone Fragility, and Bone Remodelling. *Bone* **2007**, *41*, 138–154. [[CrossRef](#)]
- Yu, E.W.; Thomas, B.J.; Brown, J.K.; Finkelstein, J.S. Simulated Increases in Body Fat and Errors in Bone Mineral Density Measurements by DXA and QCT. *J. Bone Miner. Res.* **2012**, *27*, 119–124. [[CrossRef](#)]
- Fuggle, N.R.; Curtis, E.M.; Ward, K.A.; Harvey, N.C.; Dennison, E.M.; Cooper, C. Fracture Prediction, Imaging and Screening in Osteoporosis. *Nat. Rev. Endocrinol.* **2019**, *15*, 535–547. [[CrossRef](#)]
- Mallio, C.A.; Vadalà, G.; Russo, F.; Bernetti, C.; Ambrosio, L.; Zobel, B.B.; Quattrocchi, C.C.; Papalia, R.; Denaro, V. Novel Magnetic Resonance Imaging Tools for the Diagnosis of Degenerative Disc Disease: A Narrative Review. *Diagnostics* **2022**, *12*, 420. [[CrossRef](#)] [[PubMed](#)]
- Mallio, C.A.; Greco, F.; Gaudino, F.; Beomonte Zobel, B.; Quattrocchi, C.C. Computed Tomography Density Changes of Bone Metastases after Concomitant Denosumab. *Skelet. Radiol.* **2023**, *52*, 1567–1575. [[CrossRef](#)] [[PubMed](#)]
- Brett, A.D.; Brown, J.K. Quantitative computed tomography and opportunistic bone density screening by dual use of computed tomography scans. *J. Orthop. Translat.* **2015**, *4*, 178–184. [[CrossRef](#)] [[PubMed](#)]
- Paggiosi, M.A.; Debono, M.; Walsh, J.S.; Peel, N.F.A.; Eastell, R. Quantitative Computed Tomography Discriminates between Postmenopausal Women with Low Spine Bone Mineral Density with Vertebral Fractures and Those with Low Spine Bone Mineral Density Only: The SHATTER Study. *Osteoporos. Int.* **2020**, *31*, 667–675. [[CrossRef](#)] [[PubMed](#)]
- Engelke, K.; Adams, J.E.; Armbrrecht, G.; Augat, P.; Bogado, C.E.; Bouxsein, M.L.; Felsenberg, D.; Ito, M.; Prevrhal, S.; Hans, D.B.; et al. Clinical Use of Quantitative Computed Tomography and Peripheral Quantitative Computed Tomography in the Management of Osteoporosis in Adults: The 2007 ISCD Official Positions. *J. Clin. Densitom.* **2008**, *11*, 123–162. [[CrossRef](#)] [[PubMed](#)]
- Li, N.; Li, X.; Xu, L.; Sun, W.; Cheng, X.; Tian, W. Comparison of QCT and DXA: Osteoporosis Detection Rates in Postmenopausal Women. *Int. J. Endocrinol.* **2013**, *2013*, 895474. [[CrossRef](#)] [[PubMed](#)]
- Löffler, M.T.; Jacob, A.; Valentini, A.; Rienmüller, A.; Zimmer, C.; Ryang, Y.-M.; Baum, T.; Kirschke, J.S. Improved Prediction of Incident Vertebral Fractures Using Opportunistic QCT Compared to DXA. *Eur. Radiol.* **2019**, *29*, 4980–4989. [[CrossRef](#)] [[PubMed](#)]
- Li, Y.; Jiang, Y.; Liu, H.; Yu, X.; Chen, S.; Ma, D.; Gao, J.; Wu, Y. A Phantom Study Comparing Low-Dose CT Physical Image Quality from Five Different CT Scanners. *Quant. Imaging Med. Surg.* **2022**, *12*, 766–780. [[CrossRef](#)]
- Lyu, T.; Zhao, W.; Zhu, Y.; Wu, Z.; Zhang, Y.; Chen, Y.; Luo, L.; Li, S.; Xing, L. Estimating Dual-Energy CT Imaging from Single-Energy CT Data with Material Decomposition Convolutional Neural Network. *Med. Image Anal.* **2021**, *70*, 102001. [[CrossRef](#)]
- Ghasemi Shayan, R.; Oladghaffari, M.; Sajjadian, F.; Fazel Ghaziyani, M. Image Quality and Dose Comparison of Single-Energy CT (SECT) and Dual-Energy CT (DECT). *Radiol. Res. Pract.* **2020**, *2020*, 1403957. [[CrossRef](#)]
- Therkildsen, J.; Thygesen, J.; Winther, S.; Svensson, M.; Hauge, E.-M.; Böttcher, M.; Ivarsen, P.; Jørgensen, H.S. Vertebral Bone Mineral Density Measured by Quantitative Computed Tomography With and Without a Calibration Phantom: A Comparison Between 2 Different Software Solutions. *J. Clin. Densitom.* **2018**, *21*, 367–374. [[CrossRef](#)]

23. Liu, Z.-J.; Zhang, C.; Ma, C.; Qi, H.; Yang, Z.-H.; Wu, H.-Y.; Yang, K.-D.; Lin, J.-Y.; Wong, T.-M.; Li, Z.-Y.; et al. Automatic Phantom-Less QCT System with High Precision of BMD Measurement for Osteoporosis Screening: Technique Optimisation and Clinical Validation. *J. Orthop. Transl.* **2022**, *33*, 24–30. [[CrossRef](#)] [[PubMed](#)]
24. Lee, D.C.; Hoffmann, P.F.; Kopperdahl, D.L.; Keaveny, T.M. Phantomless Calibration of CT Scans for Measurement of BMD and Bone Strength—Inter-Operator Reanalysis Precision. *Bone* **2017**, *103*, 325–333. [[CrossRef](#)] [[PubMed](#)]
25. Xiongfeng, T.; Cheng, Z.; Meng, H.; Chi, M.; Deming, G.; Huan, Q.; Bo, C.; Kedi, Y.; Xianyue, S.; Tak-Man, W.; et al. One Novel Phantom-Less Quantitative Computed Tomography System for Auto-Diagnosis of Osteoporosis Utilizes Low-Dose Chest Computed Tomography Obtained for COVID-19 Screening. *Front. Bioeng. Biotechnol.* **2022**, *10*, 856753. [[CrossRef](#)] [[PubMed](#)]
26. Lee, Y.H.; Kim, J.J.; Jang, I.G. Patient-Specific Phantomless Estimation of Bone Mineral Density and Its Effects on Finite Element Analysis Results: A Feasibility Study. *Comput. Math. Methods Med.* **2019**, *2019*, 4102410. [[CrossRef](#)] [[PubMed](#)]
27. Mueller, D.K.; Kutscherenko, A.; Bartel, H.; Vlassenbroek, A.; Ourednicek, P.; Erckenbrecht, J. Phantom-Less QCT BMD System as Screening Tool for Osteoporosis without Additional Radiation. *Eur. J. Radiol.* **2011**, *79*, 375–381. [[CrossRef](#)] [[PubMed](#)]
28. Pickhardt, P.J.; Lee, L.J.; Muñoz del Rio, A.; Lauder, T.; Bruce, R.J.; Summers, R.M.; Pooler, B.D.; Binkley, N. Simultaneous Screening for Osteoporosis at CT Colonography: Bone Mineral Density Assessment Using MDCT Attenuation Techniques Compared with the DXA Reference Standard. *J. Bone Miner. Res.* **2011**, *26*, 2194–2203. [[CrossRef](#)] [[PubMed](#)]
29. Weaver, A.A.; Beavers, K.M.; Hightower, R.C.; Lynch, S.K.; Miller, A.N.; Stitzel, J.D. Lumbar Bone Mineral Density Phantomless Computed Tomography Measurements and Correlation with Age and Fracture Incidence. *Traffic Inj. Prev.* **2015**, *16*, S153–S160. [[CrossRef](#)] [[PubMed](#)]
30. Pan, Y.; Zhao, F.; Cheng, G.; Wang, H.; Lu, X.; He, D.; Wu, Y.; Ma, H.; Hu, L.; Yu, T. Automated Vertebral Bone Mineral Density Measurement with Phantomless Internal Calibration in Chest LDCT Scans Using Deep Learning. *Br. J. Radiol.* **2023**, *96*, 20230047. [[CrossRef](#)]
31. Di, M.; Weng, Y.; Wang, G.; Bian, H.; Qi, H.; Wu, H.; Chen, C.; Dou, Y.; Wang, Z.; Ma, X.; et al. Cortical Endplate Bone Density Measured by Novel Phantomless Quantitative Computed Tomography May Predict Cage Subsidence More Conveniently and Accurately. *Orthop. Surg.* **2023**, *15*, 3126–3135. [[CrossRef](#)]
32. Henzler, T.; Fink, C.; Schoenberg, S.O.; Schoepf, U.J. Dual-Energy CT: Radiation Dose Aspects. *Am. J. Roentgenol.* **2012**, *199*, S16–S25. [[CrossRef](#)] [[PubMed](#)]
33. Lu, G.M.; Zhao, Y.; Zhang, L.J.; Schoepf, U.J. Dual-Energy CT of the Lung. *Am. J. Roentgenol.* **2012**, *199*, S40–S53. [[CrossRef](#)] [[PubMed](#)]
34. Greffier, J.; Si-Mohamed, S.; Guiu, B.; Frandon, J.; Loisy, M.; de Oliveira, F.; Douek, P.; Beregi, J.-P.; Dabli, D. Comparison of Virtual Monoenergetic Imaging between a Rapid Kilovoltage Switching Dual-Energy Computed Tomography with Deep-Learning and Four Dual-Energy CTs with Iterative Reconstruction. *Quant. Imaging Med. Surg.* **2022**, *12*, 1149–1162. [[CrossRef](#)] [[PubMed](#)]
35. Dubief, B.; Avril, J.; Pascart, T.; Schmitt, M.; Loffroy, R.; Maillefert, J.-F.; Ornetti, P.; Ramon, A. Optimization of Dual Energy Computed Tomography Post-Processing to Reduce Lower Limb Artifacts in Gout. *Quant. Imaging Med. Surg.* **2022**, *12*, 539–549. [[CrossRef](#)] [[PubMed](#)]
36. Gruenewald, L.D.; Koch, V.; Martin, S.S.; Yel, I.; Eichler, K.; Gruber-Rouh, T.; Lenga, L.; Wichmann, J.L.; Alizadeh, L.S.; Albrecht, M.H.; et al. Diagnostic Accuracy of Quantitative Dual-Energy CT-Based Volumetric Bone Mineral Density Assessment for the Prediction of Osteoporosis-Associated Fractures. *Eur. Radiol.* **2022**, *32*, 3076–3084. [[CrossRef](#)] [[PubMed](#)]
37. Nickoloff, E.L.; Feldman, F.; Atherton, J. V Bone Mineral Assessment: New Dual-Energy CT Approach. *Radiology* **1988**, *168*, 223–228. [[CrossRef](#)] [[PubMed](#)]
38. Booz, C.; Noeske, J.; Albrecht, M.H.; Lenga, L.; Martin, S.S.; Yel, I.; Huizinga, N.A.; Vogl, T.J.; Wichmann, J.L. Diagnostic Accuracy of Quantitative Dual-Energy CT-Based Bone Mineral Density Assessment in Comparison to Hounsfield Unit Measurements Using Dual X-ray Absorptiometry as Standard of Reference. *Eur. J. Radiol.* **2020**, *132*, 109321. [[CrossRef](#)]
39. Wichmann, J.L.; Booz, C.; Wesarg, S.; Bauer, R.W.; Kerl, J.M.; Fischer, S.; Lehnert, T.; Vogl, T.J.; Khan, M.F.; Kafchitsas, K. Quantitative Dual-Energy CT for Phantomless Evaluation of Cancellous Bone Mineral Density of the Vertebral Pedicle: Correlation with Pedicle Screw Pull-out Strength. *Eur. Radiol.* **2015**, *25*, 1714–1720. [[CrossRef](#)]
40. Nelson, G.S. Bias in Artificial Intelligence. *N. C. Med. J.* **2019**, *80*, 220–222. [[CrossRef](#)]
41. Dimai, H.P. New Horizons: Artificial Intelligence Tools for Managing Osteoporosis. *J. Clin. Endocrinol. Metab.* **2023**, *108*, 775–783. [[CrossRef](#)]
42. Alkaissi, H.; McFarlane, S.I. Artificial Hallucinations in ChatGPT: Implications in Scientific Writing. *Cureus* **2023**, *15*, e35179. [[CrossRef](#)]
43. Mallio, C.A.; Radbruch, A.; Deike-Hofmann, K.; van der Molen, A.J.; Dekkers, I.A.; Zaharchuk, G.; Parizel, P.M.; Beomonte Zobel, B.; Quattrocchi, C.C. Artificial Intelligence to Reduce or Eliminate the Need for Gadolinium-Based Contrast Agents in Brain and Cardiac MRI. *Investig. Radiol.* **2023**, *58*, 746–753. [[CrossRef](#)]
44. Greco, F.; Salgado, R.; Van Hecke, W.; Del Buono, R.; Parizel, P.M.; Mallio, C.A. Epicardial and Pericardial Fat Analysis on CT Images and Artificial Intelligence: A Literature Review. *Quant. Imaging Med. Surg.* **2022**, *12*, 2075–2089. [[CrossRef](#)]
45. Yu, K.-H.; Kohane, I.S. Framing the Challenges of Artificial Intelligence in Medicine. *BMJ Qual. Saf.* **2019**, *28*, 238–241. [[CrossRef](#)]
46. Zhang, Q.; Burrage, M.K.; Shanmuganathan, M.; Gonzales, R.A.; Lukaschuk, E.; Thomas, K.E.; Mills, R.; Leal Pelado, J.; Nikolaidou, C.; Popescu, I.A.; et al. Artificial Intelligence for Contrast-Free MRI: Scar Assessment in Myocardial Infarction Using Deep Learning-Based Virtual Native Enhancement. *Circulation* **2022**, *146*, 1492–1503. [[CrossRef](#)]

47. Gao, L.; Jiao, T.; Feng, Q.; Wang, W. Application of Artificial Intelligence in Diagnosis of Osteoporosis Using Medical Images: A Systematic Review and Meta-Analysis. *Osteoporos. Int.* **2021**, *32*, 1279–1286. [[CrossRef](#)] [[PubMed](#)]
48. Yang, J.; Liao, M.; Wang, Y.; Chen, L.; He, L.; Ji, Y.; Xiao, Y.; Lu, Y.; Fan, W.; Nie, Z.; et al. Opportunistic Osteoporosis Screening Using Chest CT with Artificial Intelligence. *Osteoporos. Int.* **2022**, *33*, 2547–2561. [[CrossRef](#)] [[PubMed](#)]
49. Xue, Z.; Huo, J.; Sun, X.; Sun, X.; Ai, S.; Zhang, L.; Liu, C. Using Radiomic Features of Lumbar Spine CT Images to Differentiate Osteoporosis from Normal Bone Density. *BMC Musculoskelet. Disord.* **2022**, *23*, 336. [[CrossRef](#)] [[PubMed](#)]
50. Ferizi, U.; Besser, H.; Hysi, P.; Jacobs, J.; Rajapakse, C.S.; Chen, C.; Saha, P.K.; Honig, S.; Chang, G. Artificial Intelligence Applied to Osteoporosis: A Performance Comparison of Machine Learning Algorithms in Predicting Fragility Fractures from MRI Data. *J. Magn. Reson. Imaging* **2019**, *49*, 1029–1038. [[CrossRef](#)] [[PubMed](#)]
51. Lee, H.; Park, S.; Kwack, K.-S.; Yun, J.S. CT and MR for Bone Mineral Density and Trabecular Bone Score Assessment in Osteoporosis Evaluation. *Sci. Rep.* **2023**, *13*, 16574. [[CrossRef](#)] [[PubMed](#)]

Disclaimer/Publisher’s Note: The statements, opinions and data contained in all publications are solely those of the individual author(s) and contributor(s) and not of MDPI and/or the editor(s). MDPI and/or the editor(s) disclaim responsibility for any injury to people or property resulting from any ideas, methods, instructions or products referred to in the content.